Klein tunneling in graphene systems under the influence of magnetic field

S. Bala Kumar, M. B. A. Jalil, and S. G. Tan

Citation: Journal of Applied Physics **114**, 084314 (2013); doi: 10.1063/1.4819799
View online: http://dx.doi.org/10.1063/1.4819799
View Table of Contents: http://scitation.aip.org/content/aip/journal/jap/114/8?ver=pdfcov
Published by the AIP Publishing

Klein tunneling in graphene systems under the influence of magnetic field

S. Bala Kumar,[1,a)] M. B. A. Jalil,[1,b)] and S. G. Tan[2]
[1]*Department of Electrical and Computer Engineering, National University of Singapore, Singapore 117576*
[2]*Data Storage Institute, (A*STAR) Agency for Science, Technology and Research, DSI Building, 5 Engineering Drive 1, Singapore 117608*

(Received 9 June 2013; accepted 14 August 2013; published online 30 August 2013)

We study Klein tunneling across a PN junction in monolayer graphene (MLG) and the AB-bilayer graphene (BLG) under the effect of a perpendicular magnetic-field (B-field). In the Klein tunneling process, normally incident electrons in MLG (BLG) are fully transmissive (reflective) upon hitting the junction barrier. When a finite B-field is applied, transmission of the normally incident electrons is suppressed in MLG over an energy range around the PN barrier height, effectively opening an energy gap. This suppression may be attributed to the magnetic deflection arising from Lorentz force, which shifts the transmission profile of the device in the transverse direction. © *2013 AIP Publishing LLC*. [http://dx.doi.org/10.1063/1.4819799]

INTRODUCTION

Klein paradox[1,2] has been one of the most exotic predictions in quantum electrodynamics, where relativistic particles become transparent to a high and wide potential barrier. Due to the chiral nature of electron's wave function in graphene systems,[3,4] and their zero-gap linear bandstructure, electrons injected at certain incident angles can transmit perfectly across a wide potential barrier, even though the barrier height is larger than the electron energy. Such analogous Klein tunneling (KT) effect is well known,[5–10] and has theoretically been studied in the monolayer graphene (MLG), AB-bilayer graphene (AB-BLG), ABA-trilayer, as well as the ABC-trilayer graphene, on single electrons as well as Gaussian wavepackets. This effect has also been experimentally shown in graphene systems.[11,12]

In this paper, we will investigate the effect of magnetic field on KT processes in graphene systems. Using the Dirac tight binding model, we study the effect of KT on both the MLG and the AB-BLG graphene systems, where electrons near the Dirac points behave as massless and massive Dirac fermions, respectively. In the absence of magnetic fields, our results show that in MLG, normal-incident (NI) electrons transmit perfectly across a PN-junction, even though the electron energy is lower than the barrier height. By contrast, NI-electrons in BLG reflect perfectly, consistent with previous studies of KT processes in graphene.[7] As external magnetic field is applied perpendicular to the graphene surfaces, the transmission of electrons with energy closer to the barrier height becomes suppressed, indicating a possible confinement effect due to the magnetic field.

STRUCTURE AND MODEL

We consider a device (shown in Fig. 1), where external gate voltage is applied such that an electric potential profile of: $U = 0$ ($U = U_0$) corresponding to $x < L/2$ ($x > L/2$) is established across the device, where L is the channel length, thus forming a PN-junction at $x = L/2$. Thus, electron within the energy range of $0 < E < U_0$ "sees" a potential barrier. In addition to the electric field, we also apply a perpendicular magnetic field (B-field) across the entire channel of $0 < x < L$. Here, we set $L = 100$ nm, and $U_0 = 0.1$ eV. The magnetic field is uniform in the central channel region, but zero in the source and drain regions. The uniform vertical field in the channel may be achieved by placing the device in a Helmholtz coil, or a sine-theta coil,[13] the latter achieving a higher degree of uniformity. The source and drain regions may be shielded from the applied field by covering these regions with either a type-I superconducting layer[10] or a high permeability material, e.g., Ni-Fe alloys (mu-metals).[14]

We use the Dirac Hamiltonian to model the electronic transport is graphene. The Hamiltonian[5,15,16] that approximately describes the lowest subbands for MLG and BLG is given by

$$H_n(k_x, k_y) = \gamma_n \begin{bmatrix} 0 & (k_x - ik_y)^n \\ (k_x + ik_y)^n & 0 \end{bmatrix}, \qquad (1)$$

where $\gamma_n = (\hbar v_F)^n / t_p^{n-1}$, the Fermi velocity, $v_F = 10^6$ m/s, and the interlayer hopping parameter, $t_p = 0.35$ eV. Throughout this paper, we use $n = 1$ (2) to refer to MLG (BLG). Note that $\varepsilon_F = \pm\gamma_n k_F^n$ are the eigenenergies of the lowest (highest) state of the conduction (valence) band, with $k_F = \sqrt{k_x^2 + k_y^2}$, being the Fermi wavevector. To study the transport properties, we apply the tight-binding method. This involves replacing k_x by $-i\nabla_x$ and discretizing the differential operator. Referring to Fig. 2, the discretization enables us to the transform a 2D graphene into a mode-dependent linear chain of points, with the onsite energy, $\alpha_n(k_y) = \gamma_n \begin{bmatrix} 0 & \alpha_n^{AB} \\ \alpha_n^{AB*} & 0 \end{bmatrix}$ and hopping energy, $\beta_n(k_y) = \gamma_n \begin{bmatrix} 0 & \beta_n^{AB} \\ \beta_n^{BA} & 0 \end{bmatrix}$ in pseudospin space, where $\alpha_1^{AB} = -i(k_y - 1/a)$, $\beta_1^{AB} = 0$, $\alpha_1^{AB} = -i(k_y - 1/a)$, $\alpha_2^{AB} = 2/a^2 - 2k_y/a - k_y^2$, $\beta_2^{AB} = -1/a^2$, and $\alpha_2^{AB} = 2/a^2 - 2k_y/a - k_y^2$, with a being the discretization constant. The PN-

a)Author to whom correspondence should be addressed. Electronic mail: brajahari@gmail.com
b)Electronic mail: elembaj@nus.edu.sg

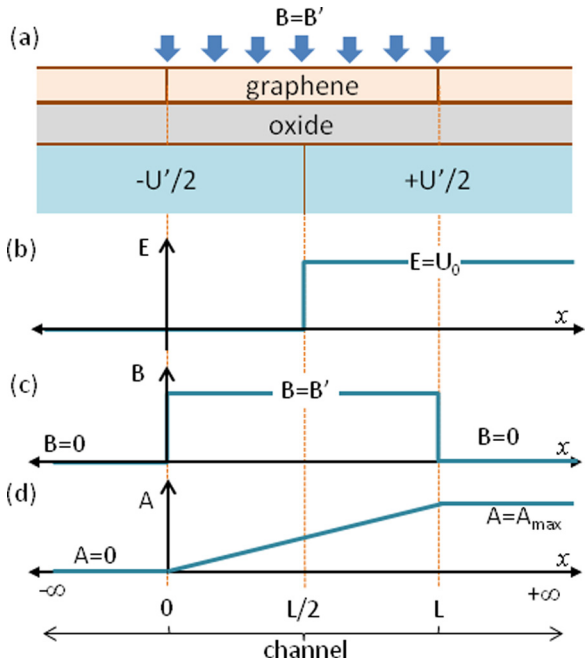

FIG. 1. (a) Device structure of a graphene under both electric and magnetic fields. (b) Electric potential profile across the graphene, forming a PN-junction at $x = L/2$. (c) B-field profile across the graphene. B-field is only applied within the channel region, i.e., $0 < x < L$. (d) The profile of the vector potential, $A = \int B(x)dx$, where $A_{\max} = BL$.

junction is modeled by adding the electric potential $U(x)$ to the onsite energy. When a constant magnetic field, B, is applied across the channel region, a vector potential of $A = \int B(x)dx$ is obtained. This effect of the B-field is reflected in the Hamiltonian[5] by replacing

$$k_y \rightarrow k_y + eA/\hbar. \tag{2}$$

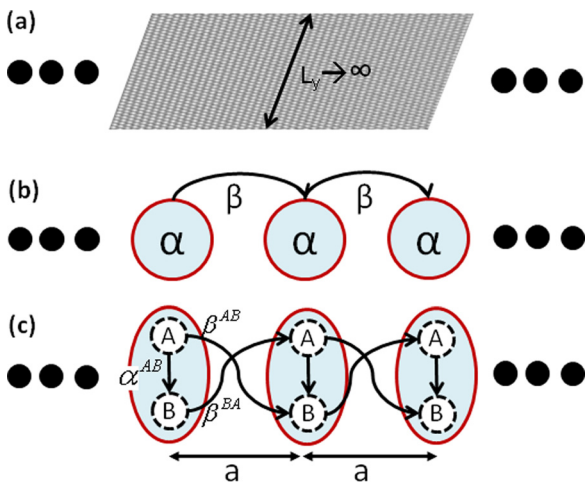

FIG. 2. (a) Infinite graphene sheet. (b) Discretization of infinite graphene layer into a linear nearest-neighbor tight binding chain. The onsite parameter, α, and hopping parameter, β, are 2×2 matrix, since each site consists of two atoms, i.e., A and B. The hopping parameters in between these atoms are shown in (c). The explicit expressions for α, β, α^{AB}, β^{AB}, and β^{BA} for both MLG and BLG are given in Eqs. (2) and (3). Note that these parameters are dependent on the values of k_y and B_Z. The distance between two neighboring sites, i.e., the discretization contacts is given by a. Here, we set $a = 5 \times 10^{-10}$ m.

As a result, the B-field modifies the mode dependent onsite energy and hopping parameter such that $\alpha_1^{AB} = -i(k_y + eA/\hbar - 1/a)$, $\alpha_2^{AB} = 2/a^2 - 2(k_y + eA/\hbar)/a - (k_y + eA/\hbar)^2$, and $\beta_2^{BA} = -1/a^2 + 2(k_y + eA/\hbar)/a$. Using the non-equilibrium Green's function formalism, we subsequently compute the electron transmission at Fermi energy, E_F for a given k_y, $T(E_F, k_y)$.

We define the transmission angle at a given $k_F = \sqrt{k_x^2 + k_y^2}$ as $\theta = \tan^{-1}(k_y/k_x)$. Note that at $k_y = 0$ (and thus $\theta = 0$), the electrons are normally incident (NI) to the barrier. We refer to the transmission of these NI electrons as T_{NI}. Based on the Hamiltonians in Eq. (1), the eigenstates of the MLG and BLG systems at k_F are given by $\psi_n^{\pm}(\theta) = \begin{bmatrix} \pm e^{in\theta} \\ 1 \end{bmatrix}$. For NI electrons, where $\theta = 0$, we have $\psi_{1,2}^{\pm}(\theta = 0) = \begin{bmatrix} \pm 1 \\ 1 \end{bmatrix} \equiv \psi^{\pm}$. Let the wavefunction of the forward-going NI electrons in the lowest (highest) energy state of the conduction (valence) band be $\psi_C(\psi_V)$. At the PN-junction, the forward going electrons are transmitted from the conduction to the valence band, and thus the wavefunction of the incident (transmitted) NI-electrons is $\psi_C(\psi_V)$.

RESULT AND DISCUSSION

We will first study the transport in a MLG system. The contour map for transmission $T(E, k_y)$ in MLG under different B-fields, is shown in Figs. 3(a)–3(c). Referring to Fig. 3, under zero B-field, perfect NI-transmission of $T_{NI} = 1$ is obtained across the PN-junction in MLG. From Eq. (1), we can show that for the MLG, $\psi_C = \psi_V = \psi^+$. As a result, the wavefunctions of the incident and transmitted NI-electrons completely overlap one another, i.e., $\langle \psi_C | \psi_V \rangle = 1$, indicating that these electrons have the same chirality. Therefore, we obtain a Klein-tunneling effect with perfect transmission of the NI-electron across the PN-junction, even though the junction barrier exceeds the electron energy.

When a finite B-field is applied, there is a distinct shift in the high transmission region of the $T(E, k_y)$ contour map. Under positive (negative) B-field, the peak transmission through the PN-junction is shifted to smaller (larger) k_y values, with the size of the shift increasing with the magnitude of the B-field. In other words, the transmission peak no longer occurs for normally incident electrons but is shifted to the left (right) of the normal axis. The strength of the shift scales with the increasing magnitude of the applied B-field. Due to this shift, NI-transmission is suppressed at the vicinity of $E = +U_0/2$, resulting in a finite energy gap for the NI-electrons. This energy gap can be understood from the physics of electron dynamics under magnetic field. Under the influence of a perpendicular B-field, electrons form circular cyclotron orbits with a well-defined radius, r_C, as shown previously by the circular trajectories of a Gaussian wavepacket in graphene under the influence of a B-field[10] As the B-field increases in strength, r_C becomes smaller. When the cyclotron diameter $d_C = 2r_C$ is smaller than the channel length, i.e., $d_C < L$, electrons are confined in the channel by

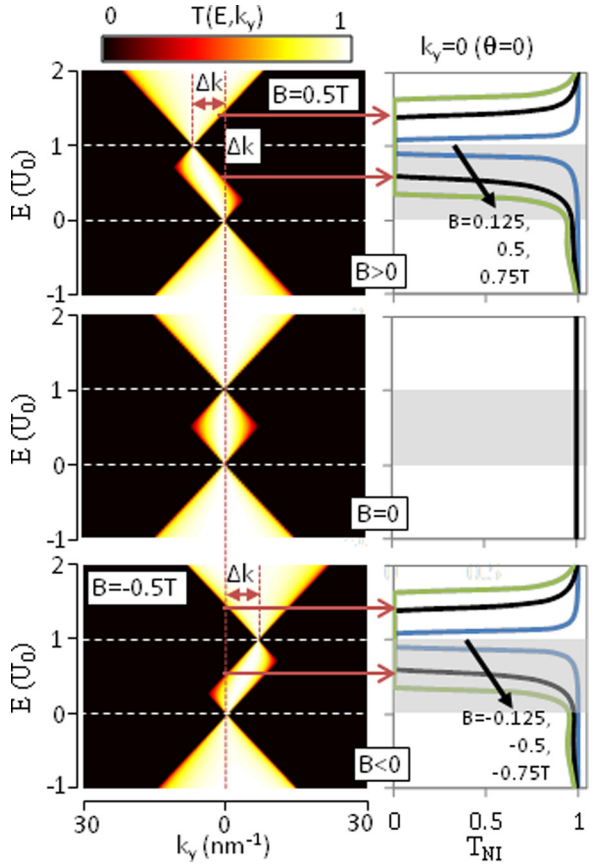

FIG. 3. (Left) T(E, k_y) map of MLG when applied B-field, B > 0, B = 0, and B < 0. The PN-junction barrier, i.e., 0 < E < U_0, is indicated by the region between the two horizontal dotted lines. Within these energy range, when B > 0 (B < 0) electron transmission region is shifted by Δk to a larger (smaller) k_y values. Thus, the T(E, k_y) map is shifted accordingly. (Right) The T_{NI} for different electron energy when B > 0, B = 0, and B < 0. The shaded region indicates the energy range of the PN-junction barrier. When B = 0, T_{NI} = 1 for all energies because of Klein tunneling. When |B| > 0, T_{NI} is suppressed to zero at around E = U_0, where U_0 is the height of the PN-junction barrier. The suppression region increases in width with increasing |B|.

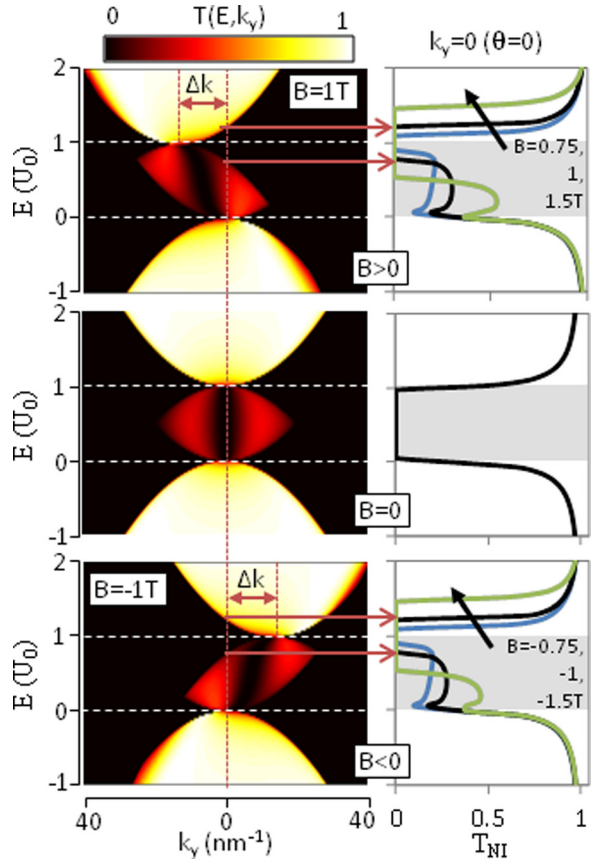

FIG. 4. (Left) T(E, k_y) map of BLG when applied B-field, B > 0, B = 0, and B < 0. The PN-junction, i.e., 0 < E < U_0, is indicated by the region between the two dotted lines. Within these energy range, when B > 0 (B < 0) the electron transmission region is shifted by Δk to a larger (smaller) k_y values. Thus, the T(E, ky) map is shifted accordingly. (Right) The T_{NI} for different electron energy when B > 0, B = 0, and B < 0. The shaded region indicates the energy range of the PN-junction. When B = 0, T_{NI} = 0 within the PN-junction and T_{NI} = 1 outside the junction barrier. When |B| > 0, T_{NI} is suppressed to zero at around E = U_0, where U_0 is the height of the PN-junction barrier. As in the MLG case, the suppression region increases in width with increasing |B|.

the circular motion, resulting in suppression of bulk transmission. The cyclotron diameter of the MLG is

$$d_{C,1} = \frac{2|E - E_D|}{eBv_F}, \tag{3}$$

where E_D is the energy at the Dirac-point. For any given B-field, d_C decreases as we approach the Dirac point, i.e., with decreasing $|E - E_D|$. Note that in a PN-junction, E_D of the transmitted electrons is located at $+U_0$. Thus, it is as if the effective B-field felt by electron is the strongest at $E = +U_0$ and this explains the suppression of T_{NI} in the vicinity of $E = +U_0$. As the applied B-field increases, transmission is further suppressed for a larger energy range about $E = +U_0$.

Unlike the case of MLG, the NI-electrons in BLG are perfectly reflected, i.e., $T_{NI} = 0$, across the PN-junction, at zero B-field (Fig. 4). From Eq. (1), we can show that for the BLG, $\psi_C = \psi^+$ and $\psi_V = \psi^-$. Thus, the wavefunctions of the incident and transmitted NI-electrons at the PN-junction have opposite chirality and are orthogonal to each other, i.e., $\langle\psi_C|\psi_V\rangle = 0$. This results in perfect reflection of NI-electrons at the PN-junction. On the other hand, the effect of B-field on the $T(E, k_y)$ map of a BLG is similar to that on MLG, i.e., the transmission peak across the PN-junction is shifted to smaller (larger) k_y values, with the size of the shift increasing with the magnitude of the positive (negative) B-field. Note that, the cyclotron diameter in BLG is

$$d_{C,2} = \frac{2\sqrt{|E - E_{dir}|t_\perp}}{eBv_F}, \tag{4}$$

and this decreases with decreasing $|E - E_{dir}|$. As in the MLG case, this results in suppression of T_{NI} in the vicinity of $+U_0/2$. For a given B-field, the effect of B-field is weaker in BLG compared to MLG.

Next, we derive the analytical expression for the electron energy range over which the T_{NI} is suppressed for both MLG and BLG. Referring to Figs. 3 and 4, when a finite B-field is applied, the transmission profile at the Dirac point of $E = U_0$ is shifted along the k_y axis by an amount Δk, which from Eq. (2), is given by

$$\Delta k = e|B|L/\hbar. \tag{5}$$

The above increases linearly with the B-field strength, and translates to an energy gap of $\varepsilon_{n,gap} = 2\gamma_n \Delta k^n$ at the vicinity of U_0 for NI electrons. In other words, transmission of NI electrons is suppressed over the energy range of $(U_0 - \varepsilon_{gap}/2) < E < (U_0 + \varepsilon_{gap}/2)$. Explicitly, the energy gap for MLG and BLG is given by $\varepsilon_{1,gap} = 2e|B|Lv_F$ and $\varepsilon_{2,gap} = 2(e|B|Lv_F)^2/t_p$, respectively.

The physics of transmission suppression discussed above corresponds directly to the angular shift of the transmission peak of the NI electrons away from normal transmission. Next, we further investigate the B-field effect on the transmission profile as a function of the electron injection-angle, θ. The transmission profiles through the PN-junction at electron energy corresponding to the mid-barrier height i.e., $E = U_0/2$, are shown in Fig. 5. At zero B-field, for the case of MLG, a finite transmission is obtained at all angles, except for electrons that travel along a direction which is completely parallel to the barrier, i.e., $\theta = \pm 90^\circ$. The transmission reaches a maximum, i.e., $T = 1$, at normal injection, i.e., $\theta = 0^\circ$, and decreases to zero with increasing angle. On the other hand, for the case of BLG, the transmission reaches maximum, i.e., $T = 1$, when $\theta = \pm 30^\circ$ and decreases to zero for both normal and parallel incidence, i.e., as $\theta \to \pm 90^\circ$ and $\theta \to 0^\circ$. Therefore, one observes two transmission peaks in the BLG when the angle of incidence is scanned from $-\pi$ to π. When B-field is applied, these transmission curves are shifted to a larger negative (positive) angle, with increasing positive (negative) B-field magnitude. This shows that by increasing B-field, electrons are deflected in the transverse direction, allowing one to select the zone (range of angles) where transmission is suppressed, or by the same token, the zone of high transmission. In other words, the Lorentz force induced by the B-field modifies the trajectory of the electrons in graphene devices, and causes the overall transmission profile to be deflected in the transverse direction.

Next, we study the effect of channel length, L on the electron transmission. Our study shows that channel length has a similar effect to the inverse of the applied B-field strength on the deflection of transmission peaks, i.e., a constant product BL results in the same extent of deflection, regardless of the individual values of B and L. Referring to Figs. 3–5, all the results can be reproduced by varying the values of B and L, as long as the product BL remains constant. It also follows that the channel length also determines the maximum B-field that can be applied before the transmission is suppressed to almost zero. When the channel length exceeds the cyclotron diameter, i.e., $L > d_C$, the bulk transmission is zero. Beyond this limit, electrons form cyclotron orbits will are confined within the channel region, resulting in a zero forward transmission. Referring to Fig. 5, when B-field strength is sufficiently large such that $L > d_C$, transmission is zero at all angles, due to the magnetic confinement of electron within the channel region.

A further analysis can be made by considering Eqs. (3), (4), and (5). By the replacement of $|E - E_{dir}| \to U_0/2$ (i.e., at the mid-barrier height), we find that bulk transmission is non-zero only when $BL < \frac{(nU_0 t_p^{n-1})^{1/n}}{ev_F}$. This is consistent with the results shown in Figs. 3 and 4. Within the PN-junction, the bulk transmission is non-zero only when $\Delta k = k'$, where $k' = 2k_F$ corresponding to $|\varepsilon_F| = |E - E_{dir}| = U_0/2$, i.e., $\Delta k = (nU_0)^{1/n}/\gamma_n$. Substituting this into Eq. (5), we can also show that the bulk transmission is non-zero only when $BL < \frac{(nU_0 t_p^{n-1})^{1/n}}{ev_F}$ for MLG and BLG, respectively, which is consistent with the above analytical result.

At energy E_F, the conductance is computed as, $G_D = g_0 \int \tau(E_F, k_y) dk_y$, where $g_0 = e^2/h$. The conductance plots for both MLG and BLG are shown in Fig. 6. For both cases, the conductance goes to zero at $E = 0$ and $E = U_0$, which is the potential barrier height. This is in agreement with Figures 3 and 4, which show that the effect of the B-field is strongest at $E = U_0$, which leads to a suppression of electron transmission for all values of k_y. Additionally, for MLG, in the energy range of $0 < E < U_0$, the conductance is maximum at the mid-barrier height ($E = U_0/2$) in the absence of B-field. This may be explained by considering the middle plot of Figure 3, which corresponds to the electron transmission in MLG at zero B-field. There is a diamond-shaped transmissive region within the energy range of $0 < E < U_0$,

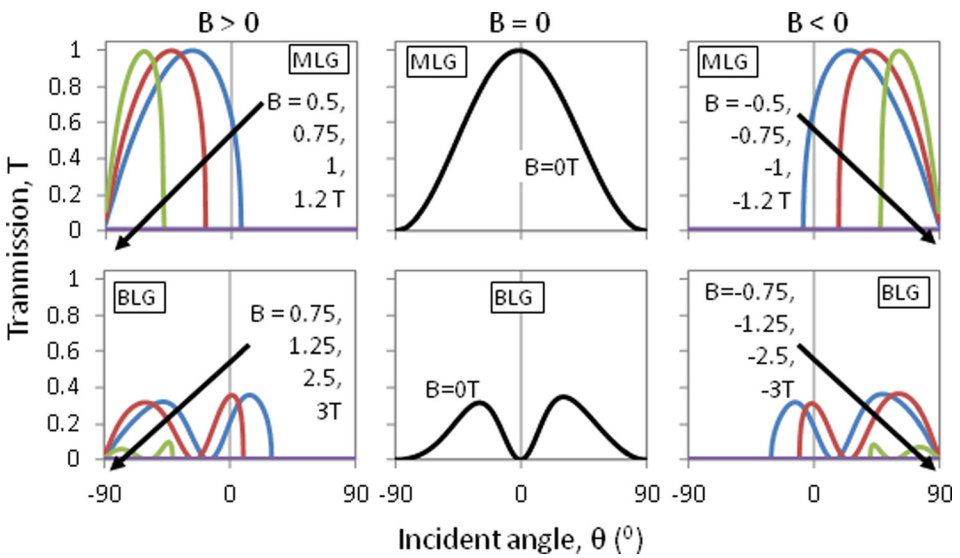

FIG. 5. The angle-dependent transmission for (top) MLG and (bottom) BLG at different B-fields. The transmission is computed at the mid-barrier height of the PN-junction, i.e., $E = U_0/2$. With increasing positive (negative) B-field, electrons are deflected to larger negative (positive) angles. When $|B|$ is large enough, such that $d_C < L$, transmission is suppressed (i.e., $T \to 0$) for all angles.

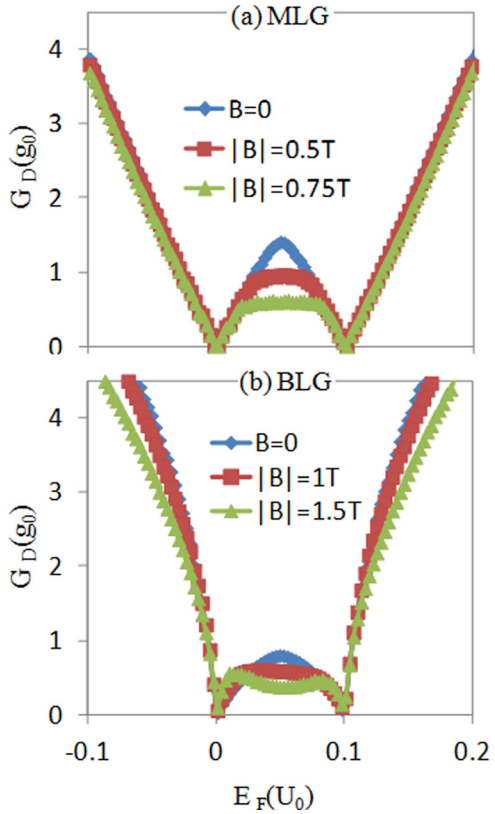

FIG. 6. Conductance across (a) MLG and (b) BLG under different B-fields.

with the transmission having the maximum extent in k_y at the mid-barrier height of $E = U_0/2$. In the presence of a B-field, the diamond shape of the high transmission region is skewed to form an oblique rectangle, which has a constant spread in k_y over a range of electron energy. This translates to the plateau in the conductance observed in the electron energy range of $0 < E < U_0$ in the presence of a finite B-field. A similar behaviour occurs for the case of BLG, but to a lesser extent due to the lower transmission values within the barrier energy range, as can be seen in Figure 4.

CONCLUSION

We have studied the Klein tunneling across the PN-junction in monolayer and bilayer graphene under a finite B-field. In the absence of a B-field, we obtain the Klein tunneling effect where NI-electrons in MLG (BLG) are completely transparent (reflective) to the PN-junction. When a finite B-field is applied, transmission is suppressed at around the barrier height, U_0. We have attributed this to the formation of the cyclotron orbits which confine the electrons within the channel region. We also showed that the transmission region is shifted along the k_y axis due to the deflection of electrons from its original angle as a result of the Lorentz force caused by the B-field. Thus, a key feature of Klein tunnelling in MLG, i.e., the perfect transmission of normally incident electrons across the PN junction no longer holds, and suppression of normally incident electrons occurs over some specific energy range. Conversely, in BLG, the total suppression of normally incident electrons is lifted in the presence of a B-field. When the B-field is sufficiently large, electrons form cyclotron orbits and are confined within the channel, leading to suppression of transmission for all incident angles. It would be interesting to extend the B-field study to the case of Klein tunneling in the presence of multiple junctions, e.g., PNP, where Fabry-Perot resonances may occur.[17]

[1]O. Klein, Z. Phys. **53**, 157 (1929).
[2]S. Ru-Keng, G. G. Siu, and C. Xiu, J. Phys. A **26**, 1001 (1993).
[3]A. H. Castro Neto, F. Guinea, N. M. R. Peres, K. S. Novoselov, and A. K. Geim, Rev. Mod. Phys. **81**, 109 (2009).
[4]A. K. Geim and K. S. Novoselov, Nature Mater. **6**, 183 (2007).
[5]C. W. J. Beenakker, Rev. Mod. Phys. **80**, 1337 (2008).
[6]V. V. Cheianov and V. I. Fal'ko, Phys. Rev. B **74**, 041403 (2006).
[7]M. I. Katsnelson, K. S. Novoselov, and A. K. Geim, Nat. Phys. **2**, 620 (2006).
[8]B. Van Duppen and F. M. Peeters, Europhys. Lett. **102**, 27001 (2013); B. Van Duppen, S. H. R. Sena, and F. M. Peeters, Phys. Rev. B **87**, 205427 (2013).
[9]M. Barbier, P. Vasilopoulos, and F. M. Peeters, Philos. Trans. R Soc. London, Ser. A **368**, 5499 (2010).
[10]Kh. Yu. Rakhimov, A. Chaves, G. A. Farias, and F. M. Peeters, J. Phys.: Condens. Matter **23**, 275801 (2011).
[11]N. Stander, B. Huard, and D. Goldhaber-Gordon, Phys. Rev. Lett. **102**, 026807 (2009).
[12]A. F. Young and P. Kim, Nat. Phys. **5**, 222 (2009).
[13]T. Katabuchi *et al.*, Rev. Sci. Instrum. **76**, 033503 (2005).
[14]R. C. O'Handley, *Modern Magnetic Materials* (John Wiley & Sons, New York, 2000), p. 25.
[15]D. P. DiVincenzo and E. J. Mele, Phys. Rev. B **29**, 1685 (1984).
[16]E. McCann and V. I. Fal'ko, Phys. Rev. Lett. **96**, 086805 (2006).
[17]M. R. Masir, P. Vasilopoulos, and F. M. Peeters, Phys. Rev. B **82**, 115417 (2010).